Laser Ultrasonics for defect evaluation on coated railway axles

Nicola Montinaro[1]*, Gabriella Epasto[2], Donatella Cerniglia[1], Eugenio Guglielmino[2]

[1] Dipartimento di Ingegneria, Università degli Studi di Palermo, Viale delle Scienze Edificio 8, 90128 Palermo, Italy.

[2] Dipartimento di Ingegneria, Università degli Studi di Messina, Contrada di Dio, Sant'Agata, 98166 Messina, Italy.

*corresponding author: nicola.montinaro@unipa.it

Keywords

Non-destructive testing; non-contact techniques; laser ultrasonic; railway axle inspection; open crack.

Abstract

This scientific paper focuses on the application of an advanced non-destructive technique for an effective inspection of railway axles. The method pertains to ultrasonic techniques, which are widely used in the railway field. The experimental investigation was carried out on simulated defects tooled near the cross section reduction of the axle, in order to simulate fatigue cracks which, due to notch effect, can trigger crack propagation and axle failure.

The aim of this research activity is to evaluate how efficiently the proposed technique detects defects and to verify its applicability to axles with a black coating for protection. In view of the experimental setup, comprising a pulsed laser for ultrasonic waves generation and a continuous beam laser plus an interferometer as the receiving unit to measure surface displacements, the presence of a black coating represents a major challenge in terms of signal detection. Nonetheless,

defects were detected by collecting all the waves in a B-scan map and data were processed by cross-reading A-scans and B-Scans in correspondence of each defect analysed. Results of the analysis show how very promising and robust the application of the proposed laser ultrasonics technique is in defect detection on painted railway axles.

1. Introduction

In the railway field, non-destructive evaluation techniques, even non-conventional ones, are a fundamental tool for on-service inspection of components, such as wheels [1–4], axles [5–8], bogies [9,10], rails [11–14] and turnouts [15].

Taking into account the nature of axle-related derailments (i.e. not related to human factor) which have occurred within the last few years [16–18], the scientific community has focused its attention on the detectability of corrosion- [19], fretting-fatigue crack [20] and fatigue-induced cracks [7,21] on axles. Fatigue cracks can initiate on the axle surface, due to the intense mechanical loads during operation. Both static and fatigue loads lead to high magnitude torsional and bending stresses. The latter ones can generate transversal surface-opened cracks which can cause stress intensification (i.e. notch effect) in specific sections of the axle (where a diameter reduction occurs), triggering fatigue crack initiation and propagation [22]. Thus, one of the main aims of the Euraxles research project [23] has become minimizing the risk of axle failure either by improving available non-destructive techniques, or by developing new ones also. The project mainly focused on ultrasonic techniques (UT) [24], which are the non-destructive techniques most widely used in the railway field [25–29]. In this regard, when visual testing (VT) reveals small defects on the surface, such as paint damage (peeling) or corrosion pits, magnetic particles testing (MT) and ultrasonic testing (UT) are the recommended inspection techniques, according to the adopted maintenance standard procedure [30]. Moreover, since ultrasonic testing is a volumetric technique, it further allows to detect internal defects and measure their effective sizes. In agreement with the aforementioned direction undertaken by the scientific community [21], in this paper the authors propose a non-conventional ultrasonic technique for defect detection on a painted solid axle, that was already successfully applied on a train wheel [31]. The main advantage of this technique lies in the use of non-contact transducers which allow more flexibility in the inspection setup (i.e. the distance between source and detector) based on the geometry of the inspected part and on the type of defect. Considering that, under a train, accessibility to the collar is very small (about 10 mm) and inspections of a train underbelly are currently performed with the train stationary in a maintenance pit line, the authors' idea is to carry out the inspection of the axle during wheelset maintenance instead, using an underfloor lathe, thus making it possible to move the train at a very low speed without any need of dismounting the wheelset. This would drastically reduce inspection time by UT. On top of that, thanks to the non-contact probes, it is not necessary to prepare the surface before inspection or to use any couplants (such as glycerine, water or gel). The proposed technique is based on a pulsed laser for ultrasonic waves generation coupled to a laser interferometer for their detection; more details can be found in [31]. The experimental campaign was carried out on a solid railway axle of the Italian Railway Company, Trenitalia SpA, coated with a new protective black paint to prevent corrosion and impact damage due to flying ballast. It is worth mentioning that several types of surface protection systems can be applied on axle surfaces [32]. The presence of a black coating represented a major challenge in using the laser – laser ultrasonics technique for inspection. Furthermore, a fine tuning of both the generating and receiving optical unit is required, the former to prevent coating damage (during ultrasonic waves generation), the latter due to the low reflectivity of black surfaces, that renders them harder to investigate by optical interferometry (during signal reception). Specifically, to ensure a negligible coating damage during ultrasonic generation, a laser line focalization was adopted (instead of a pointwise one), without multiple shots for each acquisition (no averaging) to reduce the power density injected in the sample and the number of laser strikes.

Some artificial defects, simulating fatigue cracks, were tooled in critical sections on the external surface of the axle, where stress intensification occurs due to diameter reduction, to the effect of wheel seats and/or to the bearing press-fit [33]. The acquired data are reported after generating a B-scan map for each defect.

Recent studies employed laser generated ultrasonic waves to detect shallow defects in thin plates [34] and in polymeric composites [35], highlighting its high spatial resolution. In [36], a finite element analysis was performed to study the propagation of laser generated ultrasonic waves in ablation regime inside a steel specimen with internal defects. As far as the authors are aware, few research papers deal with the application of the proposed technique in the railway field [4,8,31,37], and those are especially focused on rails defect detection [38–40]. The main differences between this research paper and previous published research [8] are two: the sample is coated and the ultrasonic waves were recorded by a laser interferometer coupled with a laser generation system instead of using non-contact air coupled ultrasonic probes. Moreover, the interferometric receiving system is equipped with a focusing lens, which can be either adjusted or substituted, if the source-detector-specimen distances or the setup geometry need to be changed; on the contrary, using air-coupled probes, such distances cannot be easily adjusted nor entirely modified.

It is worth mentioning that it is the first time the proposed technique is applied on a painted axle, whereas other non-destructive techniques are currently being developed to avoid the issue of wheelset dismounting and paint removing [41,42].

Thus, the main novelty of this research is the application of technique for defect detection on solid railway axle. The aim of this research activity is to evaluate whether the laser-laser ultrasonics technique is capable of detecting artificially created defects and to verify its efficacy and reliability in inspecting axles with a black coating for protection.

2. Experiments

2.1 Railway axle sample

A portion of a railway axle, provided by the Italian railway company Trenitalia SpA, was adopted as benchmark to prove the efficacy of the proposed non-contact UT inspection methodology. The sample axle is made in EA1N steel grade and presents a set of two reproduced superficial defects (A and B) spaced by an angle of $\pi/2$, with known geometries and positions. In Figure 1 a 3D CAD model of the axle is shown, generated by reverse engineering. The axial position of the reproduced defects fits a real case scenario of most likely locations found during worksite inspection on trains. The defects were obtained by means of a rotating saw-cut in order to produce a convex shape, which is very similar to a fatigue crack. Nevertheless, the dimensions, in terms of axial width (1 mm) and radial depth (3 mm) were designed in Trenitalia laboratories to generate an equivalent defect to be used for calibration of an ultrasonic inspection system. The UT system is equipped with a rotating probe with angled transducers for defect detection in the critical areas of axles (i.e. geometrical transitions and press-fit seats) and it is designed for testing solid axles from end faces. It is worth mentioning that the position of the defects along the axle in this study (200 mm and 280 mm) from the end face are similar to those used during the calibration of such probes (which, obviously, can change depending on the specific geometry of the axle). The depth of the defects is similar to what found in other studies [25,43,44]. Specifically, defect A lies on the journal of the axle which, in the case of an in-site inspection, would be covered by the rolling bearing, whereas defect B lies on the fillet between the collar and the wheel seat (see Figure 1). The axle is coated with a protective black paint, used to prevent corrosion and impact damage due to any flying ballast.

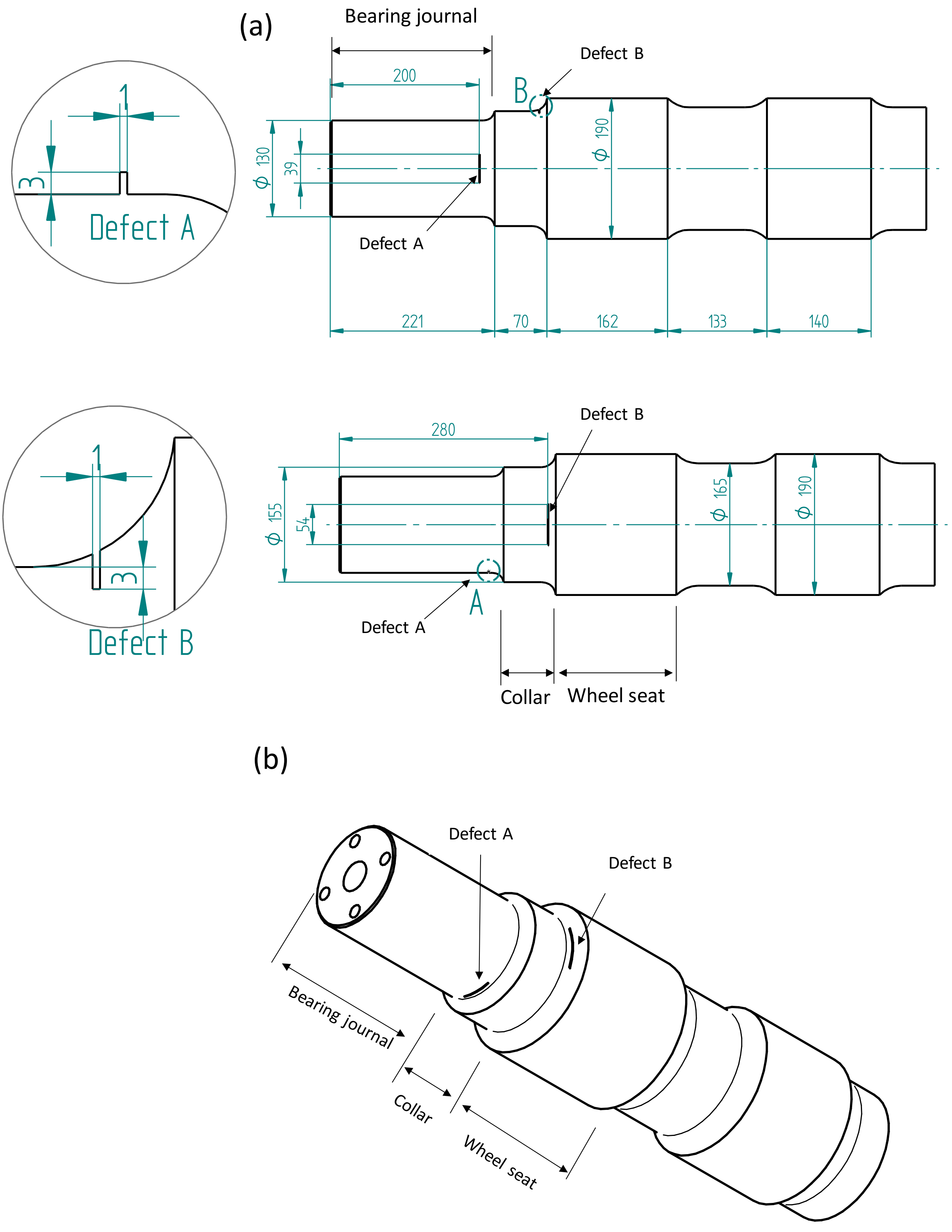

Figure 1 – Draft of the railway axle with dimensions and positions of the artificial defects (a); 3D view of the axle (b).

2.2 Experimental UT setup

An experimental preliminary study of the setups that would allow defect inspection was necessary to carry out an application of the innovative full optical ultrasonic inspection system to the painted axle.

Two different experimental setups were selected for the inspection of defects A and B: a transmission and a reflection setup, respectively. Schematics and pictures for both setups are shown in Figure 2.

In both cases, a pulsed IR Nd:YAG laser is used to generate an ultrasonic signal while a continuous wave laser combined with an interferometer is the receiving end for surface out-of-plane displacements. The acquired signal is digitized by a National Instrument® A/D converter, triggered by the generating laser, then transferred to a PC for data storage and post-processing analysis.

The axle is safely mounted in a vertical position on a motorized spindle, controlled by a PC interface. To perform the scan, the PC interface triggers the laser pulse and, after storing the UT signal from the laser receiver (by the A/D acquisition board), it moves the spindle in position for the next acquisition (as shown in Figure 2). The described loop is automatic and fairly quick, being completed in $1\ s$ ($f = 1\ Hz$).

In Table 1, 2 and 3 the specifications for the laser generator, the laser receiver and the acquisition board are summarized.

Both laser source and receiver, along with their respective optics, are mounted on an optical bench; the distance between sample and generation/receiving lasers can be varied according to accessibility needs by adjusting the focusing lenses, thus overcoming any encumbrance issues due to equipment size.

A cylindrical lens is adopted for the pulsed laser focus over the sample surface in both setups, in order to favour the UT propagation in the direction normal to the focus line (the axial direction). The linear focus reduces the power density injected in the sample surface, avoiding surface degradation. Moreover, only one shot for each acquisition was needed to generate B-scan maps (no averaging).

The length of the focused line is about *3 mm*, way shorter than any defect lengths. The laser receiver was focused in a point on the sample surface, adopting a spherical lens. The low reflectivity of the axle matt black paint required a fine focalisation of the receiver beam in order to obtain a good signal/noise ratio. For this reason, the adoption of a self-centring spindle for axle movement proved fundamental to maintain the focus of the laser interferometer during the entire rotation, without reducing the signal amplitude.

Regarding the inspection of defect B, in the reflection setup, a distance of *24 mm* was set between the source and receiving (S-R) focused beams (see Figure 3b).

The laser pulse generates longitudinal (*Lw*), shear, and surface (*Sw*) waves into the sample. A study on the UT angular propagation in the laser regimes can be found in [45].

Pulsed Laser	Type	Pulsed IR Nd:YAG
	Wavelength	1064 nm
	Energy	100 mJ
	Pulse duration	8.5 ns
	Generated bandwidth	1 – 50 MHz
	Beam diameter	4 mm
	Max pulse frequency	20 Hz

Table 1 – Laser source specifications.

Laser Receiver	Type	Continuous wave
	Wavelength	532 nm
	Power	1 W
	Optical stand-off	200 mm
	Detection bandwidth	1 – 50 MHz
	Beam diameter	~0.2 mm

Table 2 – Laser receiver specifications.

Digitizer	Brand	National Instrument® PCI 5152
	N° of channel	2
	Memory	64 Mb/Channel

	Real-time sampling	Up to 2 GS/s
	Bandwidth	Up to 300 MHz
	Impedance	From 50 Ω to 1 MΩ

Table 3 – Acquisition board specifications.

In Figure 3 a schematic representation of the wave paths for the transmission setup (Figure 3a) and reflection setup (Figure 3b) is shown.

In order to fit the strict accessibility conditions below a real train, the flexibility in the source and receiver positioning of the full optical laser-laser UT system (in respect to the more conventional UT probe) represent a unique feature. This technique could be applied in the reflection mode on the collar instead of conventional UT or rotating UT probe. In the reflection setup, both source and receiver are placed on the same side of the defect, on the collar free surface, which is accessible for inspection.

However, for defect A inspection this condition was not applicable because the laser receiver could not be focused on a curved, black painted surface (the fillet). For this reason, a transmission setup was preferred instead. In Figure 3a and 3b *iSw* and *iLw* indicate the incident surface wave and longitudinal wave, respectively.

In the transmission setup (Figure 3a and 3c), defect detection is based on the monitoring of the transmitted surface wave (*iSw*), as generated by the pulsed laser near the fillet between the journal and the collar. In particular, defect A, being in this case interposed between source and receiver, acts as a barrier for the *iSw*, neglecting its acquisition by the receiver (see Figure 3c). Thus, the transmission setup only gives information about the angular extension of the defect, not about its axial position.

In the presence of a bearing (or wheel), there is an attenuation of the surface wave at the axle, in correspondence of the contact point between axle and bearing (or wheel), since part of the surface wave will disperse to the bearing (or wheel) [37]. In this case, it would be sensible to increase the wave amplitude, so that even considering the attenuation caused by the press-fit, it remains distinguishable from the background noise. An experimental inspection with this boundary condition, adopting a laser generation and an air-coupled probe detection, can be found in [44].

As already mentioned, for defect B detection, a reflection setup was adopted instead. In the reflection setup, the defect signature is based on the monitoring of the surface wave as reflected by the defect edge (*RSw*), see Figure 3b and 3d. The adoption of the reflection setup allows to characterize defect B in terms of both circumferential length and position.

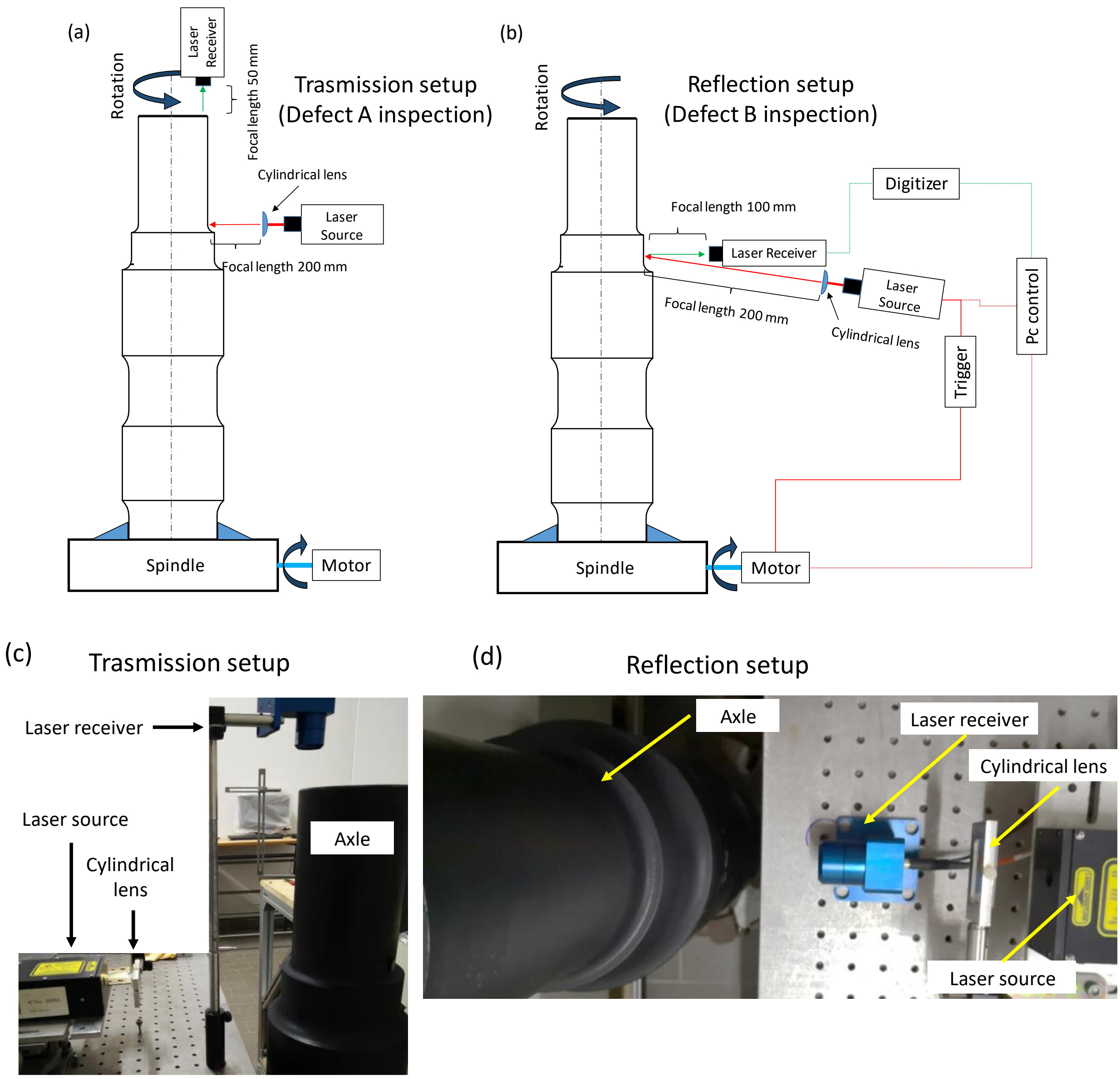

Figure 2 – Schematic representation and pictures of the experimental setup in transmission, for the inspection of Defect A (a) and (c) and in reflection, for the inspection of Defect B (b) and (d).

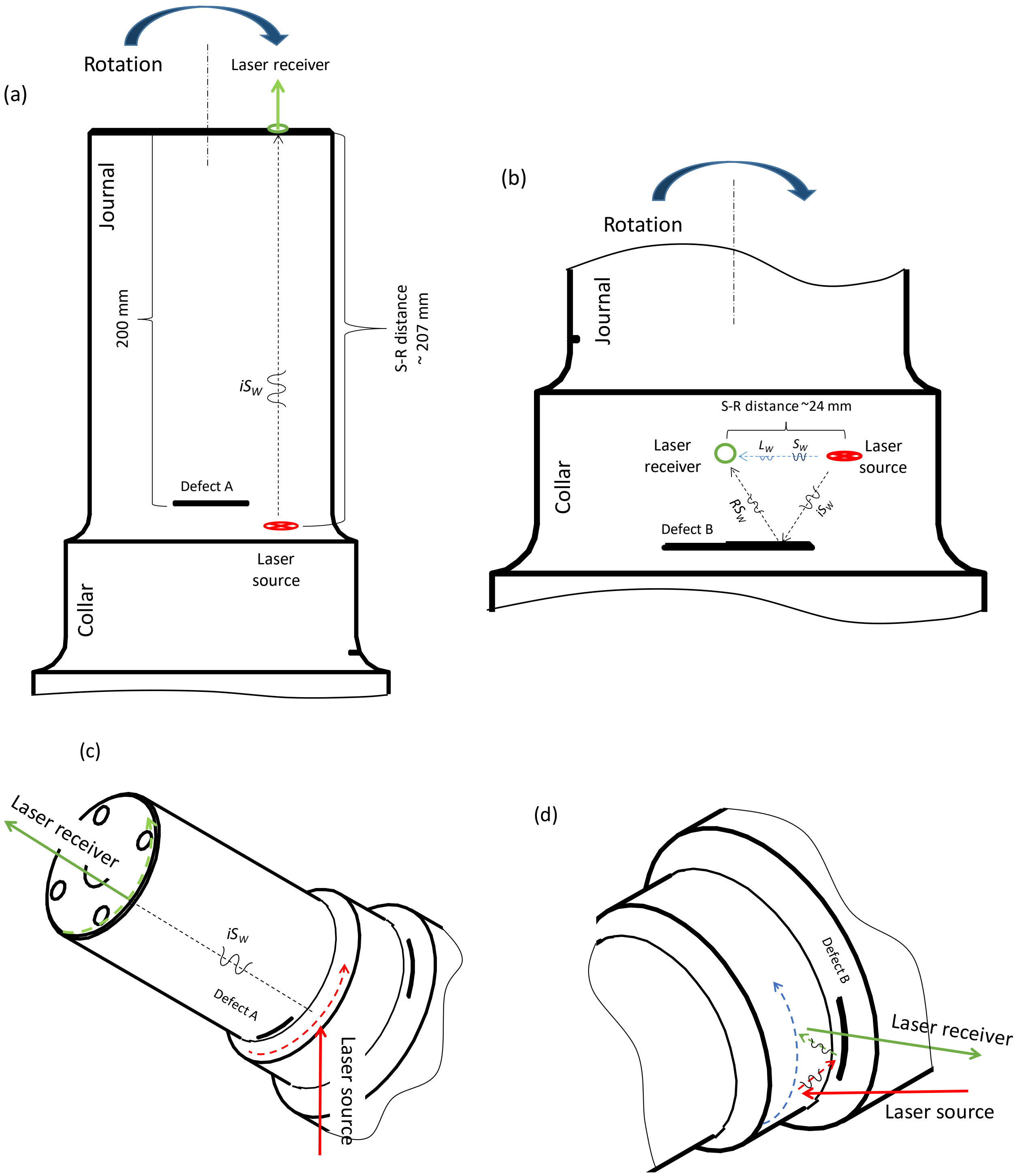

Figure 3 – Schematic representation of the surface wave paths on the axle; in (a) and (c) the transmission setup wave paths, in (b) and (d) the reflection setup wave paths.

3. Results

In this section, results of data analysis are presented, by comparing the A-Scan signals acquired in sound and defected zone, together with a B-scan map generated by stacking up the A-scan acquisitions. To generate the B-scan, the axle is rotated in fixed angular steps for each acquisition.

All the A-scan signals are post-processed by applying a time truncation window, a noise reduction filter (s) and an amplitude signal normalization, before being stacked up and plotted in the B-scan map. The abscissa and ordinate of the B-scan indicate, respectively, the time and laser position; signal amplitude is represented by a rainbow colour based scale.

3.1 Defect A

The possibility of inspecting the external part of the axle journal is created by using the transmission setup (see Figure 3c). The surface wave is generated close to the fillet radius, with the laser source - laser receiver distance being about *207 mm*. The laser source is linearly focused on the axle surface, along the circumferential direction. The distance between the laser source and defect A is equal to *6 mm*, while the circumferential length of defect A is *39 mm* (see Figure 1a). The axle is rotated in angular steps of *4.5°* degrees for each acquisition.

The A-scan signals are post-processed by applying a time truncation window of *100 µs* and a band-pass filter between *1 MHz* and *2 MHz* to reduce any noise mainly due to the relatively high S-R distance (see Figure 4).

The B-scan map for defect A is shown in Figure 4a. Considering the surface wave speed in steel ($v_s=2.8\ mm/\mu s$), the time-of-flight of the *iSw* is in agreement with what observed in Figure 4a, relatively to the sound zone, and equal to *~74 µs*. A background noise is still visible, even though it does not affect the detection of the surface wave.

The defect signature can be clearly identified by the interruption of the *iSw* in the map (see Figure 4a). Actually, the defect acts as a barrier for the *Sw* traveling between the laser source and receiver, thus such an interruption is a direct proof of the defect angular position on the surface (see Figure 4c). If the defect were shorter in length than the width of the laser source (*3 mm*), a reduction of the surface wave instead of a complete interruption would be observed. Starting from the angular extension α of the *iSw* interruption, it is also possible to estimate the circumferential length of defect A, l_A, by using the geometric formula $l_A = \alpha_A \frac{d_1}{2}$, with d_1 being the diameter of the journal (d_1 = *130 mm*), where defect A lies (see Figure 1a). By this formula, we obtain an estimated length of l_A=*30.6 mm*, underestimating the real defect length of *39 mm*. This difference could be due to two factors:

- the resolution of the step by step acquisition (*4.5°*) which adds a significant instrument error, up to *5.1 mm* (for journal diameter);
- the linear focalization length of *3 mm* which could lead to a partial interruption of the *iSw* in the proximity of the two defect ends (due to the partial transmission of the signal).

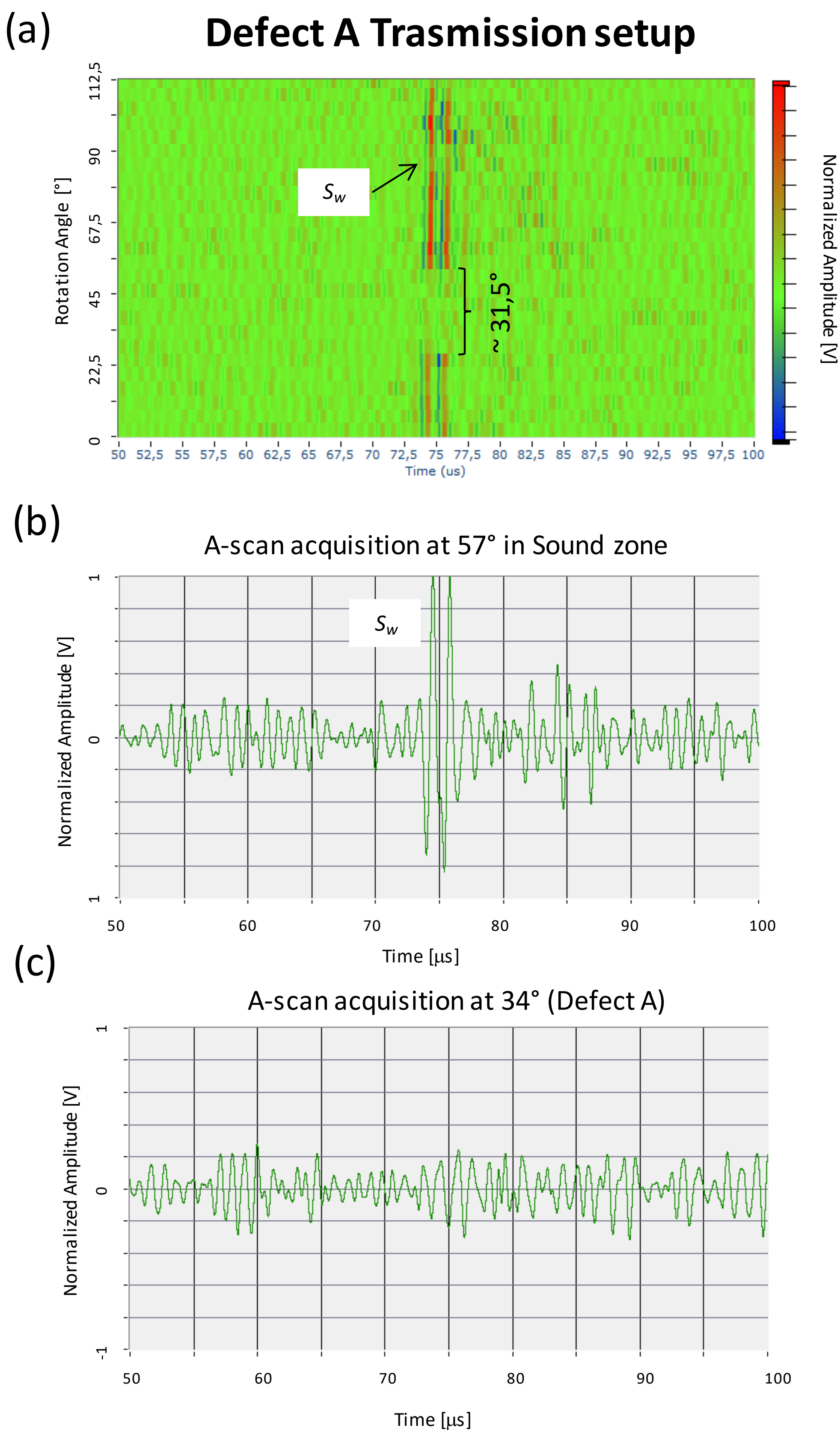

Figure 4 – B-Scan image of the defected area obtained with the transmission setup (a); A-scan signals acquired on sound zone (b) and over defect A (c).

3.2 Defect B

The inspection of the collar is made by adopting the reflection setup (see Figure 3d). The pulsed laser simultaneously generates all the types of waves in the medium (longitudinal, superficial and transversal) but, for defect detection, only the reflected surface wave (*RSw*), needs to be monitored. The S-R distance is *24 mm* (see Figure 5d or 3b), while the laser source is linearly focused on the axle surface, along the circumferential direction (with *3 mm* length). The circumferential length of defect B, located on the fillet of the collar, is *54 mm* (see Figure 1b). The axle is rotated in half steps of *4.5°/2* degrees for each acquisition.

The A-scan signals are post-processed by applying a time truncation window of *25 μs* and a *3 MHz* low-pass filter of the 2nd order, to reduce the noise on the high frequency end. In Figure 5a the B-scan of the defected B zone is shown.

Considering the longitudinal and surface wave speed in steel ($v_l=5.85\ mm/\mu s$ and $v_s=2.8\ mm/\mu s$), the time-of-flight for the *Lw* and *Sw* travelling in the S-R direction (see the blue arrow in Figure 5d) are in agreement with what observed in the A-scan of Figure 5b, relatively to the sound zone, and equal to $t_l = 24/5.85 = 4.1\ \mu s$ and $t_s=24/2.8 = 8.6\ \mu s$, respectively. The same *Lw* and *Sw* are visible in the B-scan map of Figure 5a in terms of vertical bands for the whole length of the acquisition.

Defect B signature can be clearly spotted by the generation of the reflected surface wave *RSw*, in the B-scan (see Figure 5a) or in the A-scan signal relatively to the defected zone (see Figure 5c).

Looking at the schematic representation of Figure 5d, the distance *d* between defect and scanline can be estimated by applying Pitagora's theorem to the triangle whose vertices are: the laser source, the laser receiver and the impact point A. Since the time-of-flight of the *Lw* and *Sw* are known, the cathetus can be calculated ($velocity \cdot time$), and the distance *d* results equal to *19.4 mm*, in line with the one measured in the experimental setup.

The circumferential length of defect B can be reconstructed with the same procedure as what explained for the superficial defect A. Starting from the angular extension α of the *RSw,* as extracted from the B-scan in Figure 5a, an estimate of the l_B can be calculated using the formula

$l_B = \alpha_B \frac{d_B}{2}$, where d_B is the diameter at the defect position. Since defect B position is on the fillet of the collar, the real d_B value is in the range $d_2 < d_B < d_3$ with d_2 and d_3 being the diameters of the collar and of the wheel seat, respectively. From the measure taken on the axle and from the 3D reconstructed model, the real d_B value is estimated to be *160 mm*, and from this, the estimated length of defect B would be $l_B = 50.3\ mm$. The obtained l_B slightly underestimates the real length of defect B, which is equal to *54 mm*.

This discrepancy could be explained with the same two factors influencing defect A length reconstruction:

- the resolution of the step by step acquisition which adds a significant error equal to *3.1 mm* (for d_b diameter);
- the linear focalization length of *3 mm* which could lead to a partial reflection of the *iSw* in the proximity of the two defect ends.

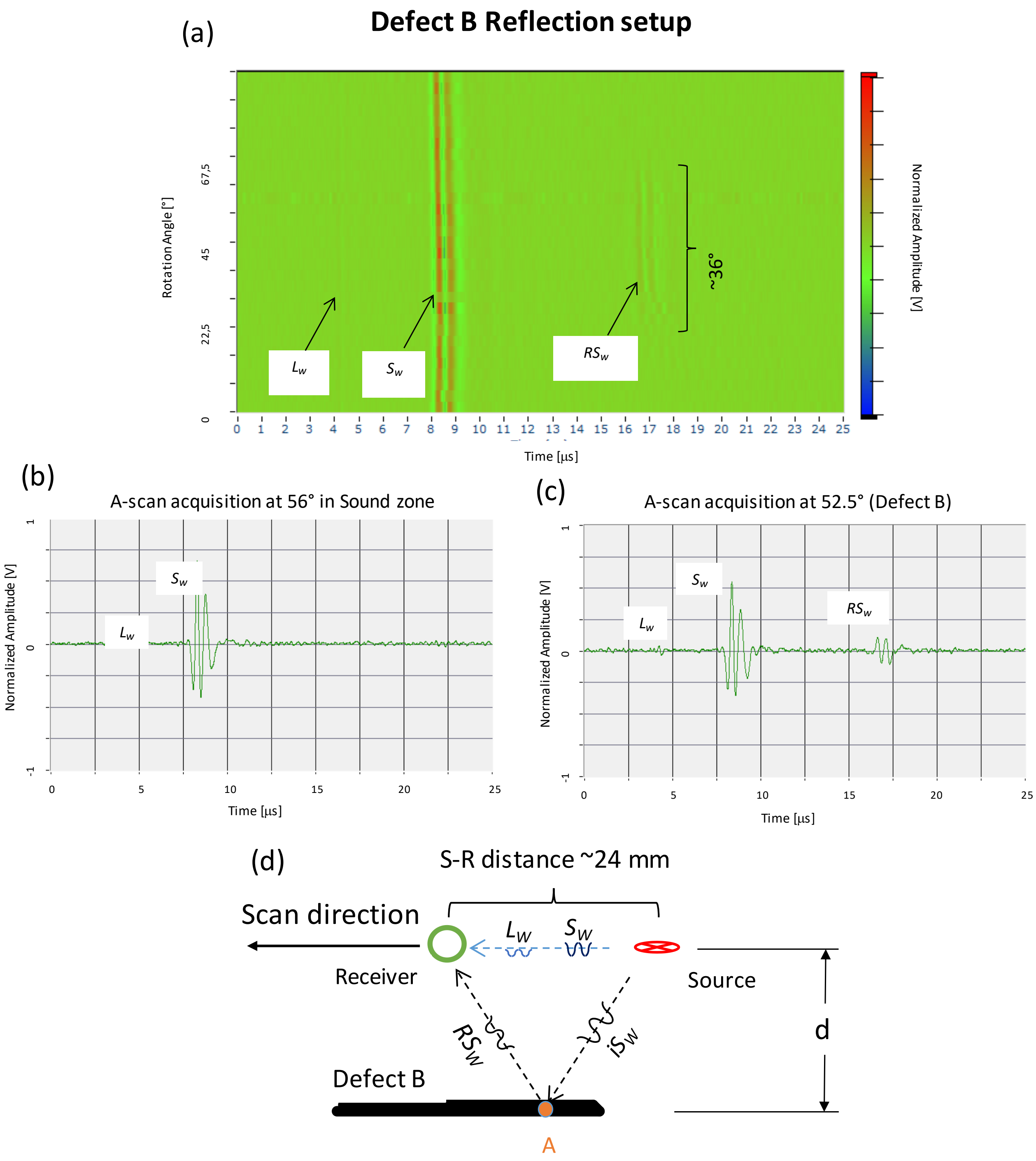

Figure 5 – B-Scan image of the of the defected area obtained with the reflection setup (a); the A-scan signals acquired

285 on sound zone (b) and over Defect B (c); schematic representation of the inspection strategy (d).

4. Conclusions

In this research paper, a non-conventional ultrasonic technique is proposed for defect detection in a painted railway axle where some artificial defects were introduced to simulate fatigue cracks in critical regions. The experimental setup is based on a pulsed laser to generate ultrasonic waves and on a laser receiver to detect them. One of the main advantages of this technique lies in the possibility of performing defect detection without dismounting the wheelset, for instance by using an underfloor lathe, when it is possible to move the train at a low speed, reducing out-of-service time for the axle. Notwithstanding, the experiments in this work are conducted in a clean laboratory setup, pointing towards further studies to be conducted before application on a real inspection site. Indeed, the authors aim to carry out the inspection of the axle during the wheelset maintenance by an underfloor lathe, making it possible to move the train at a very low speed and getting rid of the need of dismounting the wheelset. In this case, this technique could be applied in reflection mode on the collar as opposed to conventional UT or rotating UT probe.

By analysing experimental results, it is possible to see how the reflection setup used for defect B detection can also be arranged to inspect the other axle sections, whereas the same cannot be done for defect A detection, since the latter is located in the axle journal (under the bearing seat). For this reason, it proved necessary to generate a transmission signal at the axle end face. However, even in this case, the transmission inspection can be easily carried out after opening the axle box and removing the bearing retaining ring, due to setup flexibility in the laser positioning.

On the other hand, during the experimental campaign, some issues arose mainly due to the presence of the protective black coating, which made it difficult to focus the reflected signals on the laser receiver. According to the authors, this aspect does not necessarily represent a limitation to the technique applicability, since different kinds of coating are generally found on axle surfaces.

To sum up, the results are quite promising and reliable, even though the experiments were conducted in a laboratory environment, thus, further study in realistic conditions, with different axle geometries and defects need to be conducted, before the technology is moved to real inspection sites.

Acknowledgements

The authors would like to thank Trenitalia Spa, “Direzione Tecnica Ingegneria Rotabili e Tecnologie di Base, Tecnologie Meccaniche e Sistemi Frenanti, Processi Speciali” and “Unità Operativa CND” and mainly Luca Labbadia, Valentina Leonardi and Marco Sarti for their support and for providing the railway axle.

References

[1] Verkhoglyad AG, Kuropyatnik IN, Bazovkin VM, Kuryshev GL. Infrared diagnostics of cracks in railway carriage wheels. Russ J Nondestruct Test 2008;44:664–8. doi:10.1134/S1061830908100021.

[2] Le M, Jun J, Kim J, Lee J. Nondestructive testing of train wheels using differential-type integrated Hall sensor matrixes embedded in train rails. NDT E Int 2013;55:28–35. doi:10.1016/j.ndteint.2013.01.003.

[3] Alemi A, Corman F, Lodewijks G. Condition monitoring approaches for the detection of railway wheel defects. Proc Inst Mech Eng Part F J Rail Rapid Transit 2017;231:961–81. doi:10.1177/0954409716656218.

[4] Cavuto A, Martarelli M, Pandarese G, Revel GM, Tomasini EP. Train wheel diagnostics by laser ultrasonics. Meas J Int Meas Confed 2016;80:99–107. doi:10.1016/j.measurement.2015.11.014.

[5] Rolek P, Bruni S, Carboni M. Condition monitoring of railway axles based on low frequency vibrations. Int J Fatigue 2016;86:88–97. doi:10.1016/j.ijfatigue.2015.07.004.

[6] Traupe M, Jenne S, Lütkepohl K, Varfolomeev I. Experimental validation of inspection intervals for railway axles accompanying the engineering process. Int J Fatigue 2016;86:44–51. doi:10.1016/j.ijfatigue.2015.09.020.

[7] Kappes W, Hentschel D, Oelschlägel T. Potential improvements of the presently applied in-service inspection of wheelset axles. Int J Fatigue 2016;86:64–76. doi:10.1016/j.ijfatigue.2015.08.014.

[8] Cavuto A, Martarelli M, Pandarese G, Revel GM, Tomasini EP. Experimental investigation by laser ultrasonics for high speed train axle diagnostics. Ultrasonics 2015;55:48–57. doi:10.1016/j.ultras.2014.08.010.

[9] Kim J. Non-Destructive Characterization of Railway Materials and Components with Infrared Thermography Technique. Materials (Basel) 2019;12:4077. doi:10.3390/ma12244077.

[10] Wei X, Chen Y, Lu C, Chen G, Huang L, Li Q. Acoustic emission source localization method for high-speed train bogie. Multimed Tools Appl 2020. doi:10.1007/s11042-019-08580-3.

[11] Zhou L, Brunskill HP, Lewis R. Real-time non-invasive measurement and monitoring of wheel–rail contact using ultrasonic reflectometry. Struct Heal Monit 2019;18:1953–65. doi:10.1177/1475921719829882.

[12] Alahakoon S, Sun YQ, Spiryagin M, Cole C. Rail Flaw Detection Technologies for Safer, Reliable Transportation: A Review. J Dyn Syst Meas Control 2018;140. doi:10.1115/1.4037295.

[13] Papaelias MP, Lugg MC, Roberts C, Davis CL. High-speed inspection of rails using ACFM techniques. NDT E Int 2009;42:328–35. doi:10.1016/j.ndteint.2008.12.008.

[14] Naeimi M, Li Z, Qian Z, Zhou Y, Wu J, Petrov RH, et al. Reconstruction of the rolling contact fatigue cracks in rails using X-ray computed tomography. NDT E Int 2017;92:199–212. doi:10.1016/j.ndteint.2017.09.004.

[15] Wang K, Cao W, Xu L, Yang X, Su Z, Zhang X, et al. Diffuse ultrasonic wave-based structural health monitoring for railway turnouts. Ultrasonics 2020;101:106031. doi:10.1016/j.ultras.2019.106031.

[16] Lin C-Y, Rapik Saat M, Barkan CP. Quantitative causal analysis of mainline passenger train accidents in the United States. Proc Inst Mech Eng Part F J Rail Rapid Transit 2019:095440971987612. doi:10.1177/0954409719876128.

[17] Klinger C, Bettge D. Axle fracture of an ICE3 high speed train. Eng Fail Anal 2013;35:66–81. doi:10.1016/j.engfailanal.2012.11.008.

[18] Islam DMZ, Laparidou K, Burgess A. Cost effective future derailment mitigation techniques for rail freight traffic management in Europe. Transp Res Part C Emerg Technol 2016;70:185–96. doi:10.1016/j.trc.2015.06.017.

[19] Yuan FQ, Lu JM. Improved condition monitoring system to protect railway axle bearing safety from electric corrosion. 2015 IEEE Int. Conf. Ind. Eng. Eng. Manag., IEEE; 2015, p. 1634–8. doi:10.1109/IEEM.2015.7385924.

[20] Amini A, Entezami M, Papaelias M. Onboard detection of railway axle bearing defects using envelope analysis of high frequency acoustic emission signals. Case Stud Nondestruct Test Eval 2016;6:8–16. doi:10.1016/j.csndt.2016.06.002.

[21] Zhu C, He J, Peng J, Ren Y, Lin X, Zhu M. Failure mechanism analysis on railway wheel shaft of power locomotive. Eng Fail Anal 2019;104:25–38. doi:10.1016/j.engfailanal.2019.05.013.

[22] Náhlík L, Pokorný P, Ševčík M, Fajkoš R, Matušek P, Hutař P. Fatigue lifetime estimation of railway axles. Eng Fail Anal 2017;73:139–57. doi:10.1016/j.engfailanal.2016.12.014.

[23] “EURAXLES”, Minimizing the risk of fatigue failure of railway axles. Available online: www.euraxles.eu, 2014.

[24] Garcia-Prada JC, Gomez MJ, Castejon C. Automatic online fatigue crack detection in railway axles. 2016 18th Int. Wheel. Congr., IEEE; 2016, p. 80–3. doi:10.1109/IWC.2016.8068372.

[25] Liaptsis D, Cooper I, Boyle K, Nicholson PI, Thompson DO, Chimenti DE. The application of phased array ultrasonic techniques for inspection of railway axles from their end face. AIP Conf. Proc., 2011, p. 1440–7. doi:10.1063/1.3592101.

[26] Peng CY, Gao XR, Wang A. Novel wavelet self-optimisation threshold denoising method in axle press-fit ultrasonic defect detection. Insight - Non-Destructive Test Cond Monit 2016;58:145–51. doi:10.1784/insi.2016.58.3.145.

[27] Belalia A, Kamla Y, Amara M, Meliani MH, El Azizi A, Azari Z. Experimental and numerical investigation of UIC 54 rail degradation. Eng Fail Anal 2019:104163. doi:10.1016/j.engfailanal.2019.104163.

[28] Yuan M, Li J, Liu Y, Gao X. Automatic Recognition and Positioning of Wheel Defects in Ultrasonic B-Scan Image Using Artificial Neural Network and Image Processing. J Test Eval 2020;48:20180545. doi:10.1520/JTE20180545.

[29] Pohl R, Erhard A, Montag HJ, Thomas HM, Wüstenberg H. NDT techniques for railroad wheel and gauge corner inspection. NDT E Int 2004;37:89–94. doi:10.1016/j.ndteint.2003.06.001.

[30] R Gallo, S Cantini DM. A new wheelset maintenance concept. World Congr. Railw. Res., 2013, p. paper no. PB012615.

[31] Montinaro N, Epasto G, Cerniglia D, Guglielmino E. Laser ultrasonics inspection for defect evaluation on train wheel. NDT E Int 2019;107:102145. doi:10.1016/j.ndteint.2019.102145.

[32] Gerlach T, Kemp-Lettkamp C. EURAXLES - A global approach for design, production and maintenance of railway axles: WP4 - “Tools, technologies and surface protection systems minimizing the negative influence of corrosion or surface damage on the free axle surface“. Materwiss Werksttech 2017;48:699–718. doi:10.1002/mawe.201600581.
[33] Grubisic V, Fischer G. Railway axle failures and durability validation. Proc Inst Mech Eng Part F J Rail Rapid Transit 2012;226:518–29. doi:10.1177/0954409712442325.
[34] Kang KC, Kim YH, Choi WY, Park KK. Measurement of shallow defects using noncontact broadband leaky Lamb wave produced by pulsed laser with ultrasound microphone. NDT E Int 2020;111:102224. doi:10.1016/j.ndteint.2020.102224.
[35] Abetew A, Truong T, Hong S, Lee J, Ihn J. Parametric optimization of pulse-echo laser ultrasonic system for inspection of thick polymer matrix composites. Struct Heal Monit 2020;19:443–53. doi:10.1177/1475921719852891.
[36] Choi S, Jhang KY. Internal defect detection using laser-generated longitudinal waves in ablation regime. J Mech Sci Technol 2018;32:4191–200. doi:10.1007/s12206-018-0817-1.
[37] Mineo C, Cerniglia D, Pantano A. Numerical study for a new methodology of flaws detection in train axles. Ultrasonics 2014;54:841–9. doi:10.1016/j.ultras.2013.10.008.
[38] Yunjie Z, Xiaorong G, Lin L, Yongdong P, Chunrong Q. Simulation of Laser Ultrasonics for Detection of Surface-Connected Rail Defects. J Nondestruct Eval 2017;36:1–10. doi:10.1007/s10921-017-0451-3.
[39] Jiang Y, Wang H, Tian G, Yi Q, Zhao J, Zhen K. Fast classification for rail defect depths using a hybrid intelligent method. Optik (Stuttg) 2019;180:455–68. doi:10.1016/j.ijleo.2018.11.053.
[40] Gonzales K, Kendarian S, Carter D, Smith A, Morgan R. Non-Contact Interrogation of Railroad Axles Using Laser-Based Ultrasonic Inspection. Jt. Rail, ASME; 2005, p. 145–50. doi:10.1115/RTD2005-70058.
[41] Chaoyong P, Grondin E, Xiaorong G, Imbert C. Solid axle defect detection technique based on phased array ultrasonics. 2016 18th Int. Wheel. Congr., IEEE; 2016, p. 29–33. doi:10.1109/IWC.2016.8068362.
[42] Wang Y, Gao X, Finckbohner M, Netzelmann U. The effect of paint coatings on detection of vertical surface cracks in metals by induction thermography. NDT E Int 2019;104:58–68. doi:10.1016/j.ndteint.2019.04.002.
[43] Gonzates K, Kendarian S, Carter D, Smith A, Morgan R. Non-contact interrogation of railroad axles using laser-based ultrasonic inspection. Proc. 2005 ASME/IEEE Jt. Rail Conf. 2005., IEEE; 2005, p. 145–50. doi:10.1109/RRCON.2005.186070.
[44] Cavuto A, Martarelli M, Pandarese G, Revel GM, Tomasini EP. Experimental investigation by Laser Ultrasonics for train wheelset flaw detection. J Phys Conf Ser 2018;1149:012015. doi:10.1088/1742-6596/1149/1/012015.
[45] C.B Scruby L. D. Laser Ultrasonics Techniques and Applications. CRC Press; 1990.